Constraining the Inclinations of Binary Mergers from Gravitational-wave Observations

S. A. Usman[ORCID], J. C. Mills[ORCID], and S. Fairhurst[ORCID]
School of Physics and Astronomy, Cardiff University, The Parade, Cardiff, CF24 3AA, UK[1]

Abstract

Much of the information we hope to extract from the gravitational-wave signatures of compact binaries is only obtainable when we can accurately constrain the inclination of the orbital plane relative to the line of sight. In this paper, we discuss in detail a degeneracy between the measurement of the binary distance and inclination that limits our ability to accurately measure the inclination using gravitational waves alone. This degeneracy is exacerbated by the expected distribution of events in the universe, which leads us to prefer face-on systems at a greater distance. We use a simplified model that only considers the binary distance and orientation and show that this gives comparable results to the full parameter estimates obtained from the binary neutron star merger GW170817. For the advanced LIGO-Virgo network, it is only binaries that are close to edge-on, i.e., with inclinations $\iota \gtrsim 75°$, that will be distinguishable from face-on systems. Extended networks that have good sensitivity to both gravitational-wave polarizations will only be able to constrain the inclination of a face-on binary at a signal-to-noise ratio of 20 to $\iota \lesssim 45°$. Even for loud signals with signal-to-noise ratios of 100, face-on signals will only be constrained to have inclinations $\iota \lesssim 30°$. In the absence of observable higher modes or orbital precession, this degeneracy will dominate the mass measurements of binary black hole mergers at cosmological distances.

Key words: binaries: general – gravitational waves – stars: black holes – stars: distances – stars: neutron

1. Introduction

With its ground-breaking detections in the first years of its operation, the upgraded Laser Interferometer Gravitational-Wave Observatory (LIGO) and Virgo detectors have opened up the door to discovering new information about the universe. The collaboration's many gravitational-wave (GW) detections from binary systems, including GW150914 (Abbott et al. 2016a) and GW170817 (Abbott et al. 2017e), have allowed us to draw new insights from these astrophysical sources. These developments include constraining the nuclear equation of state (De et al. 2018) and constraining binary black hole (BBH) populations (Farr et al. 2017; Tiwari et al. 2018; Roulet & Zaldarriaga 2019). With more detections, we hope to learn even more about our universe and obtain information such as more accurate measurements of the Hubble constant H_0 (Schutz 1986; Abbott et al. 2017a) or more detailed measurements of the opening angles for gamma-ray bursts (GRBs) from binary neutron star systems (BNS; Clark et al. 2015; Goldstein et al. 2017; Metzger 2017). However, both of these values rely on the accurate measurement of the distance to the binaries and the inclination of their orbital angular momentum with respect to the line of sight. A degeneracy exists between distance and inclination, making the measurement of these two parameters very difficult. Of the compact binary detections made by LIGO and Virgo, only the BNS merger GW170817 has had a tightly constrained inclination and distance. The detection of a kilonova afterglow allowed for an accurate distance measurement (Tanvir et al. 2017; Villar et al. 2017), breaking the degeneracy with inclination. When this type of external information is unavailable, the degeneracy severely limits our ability to measure these parameters.

In this paper, we will show that this degeneracy is typical for binary mergers. The measured amplitude and phase of the GW signal encode the properties of the binary. In particular, it is the differing amplitude of the two polarizations of the gravitational waveform that allow us to determine the binary inclination.

However, the plus $(+)$ and cross $(\times)$ polarizations have nearly identical amplitudes at small inclination angles (less than $45°$) and significantly lower amplitudes at large inclination angles (greater than $45°$). This leads to two simple observations. First, the signal is strongest for binaries that are close to face-on $(\iota \sim 0°)$ or face-away $(\iota \sim 180°)$ and thus we will be observationally biased toward detecting binaries whose orbital angular momentum is well-aligned (or anti-aligned) with the line of sight (Nissanke et al. 2010; Schutz 2011). Second, for small angles, the amplitudes of the two polarizations are close to equal and we cannot measure distance or inclination separately. Therefore, for the majority of detections, this face-on degeneracy will limit our ability to constrain both electromagnetic (EM) emission models and the Hubble constant. There are various ways to break this degeneracy, such as using the EM-measured distance or using jet modeling to constrain the opening angle. These techniques were used to improve the constraints on the inclination and distance for the BNS merger GW170817 (Guidorzi et al. 2017; Abbott et al. 2018; Cantiello et al. 2018; Finstad et al. 2018; Mandel 2018).

Since an inclined binary system would produce both a high-amplitude plus polarization and a lower-amplitude cross polarization, creating a network of detectors that is sensitive to both the plus and cross-polarization has been suggested to constrain the inclination using only GWs (Blair et al. 2008). A single L-shaped detector is sensitive to just one polarization of a GW. Hanford and Livingston are almost aligned and see essentially the same polarization, while Virgo is anti-aligned and is sensitive to the orthogonal polarization. The addition of KAGRA (Aso et al. 2013) and LIGO-India (Sathyaprakash et al. 2013) would further increase the network's sensitivity to the orthogonal polarization. Thus, it is hoped that this five-detector network could better constrain the inclination angle and distance. We examine this possibility of constraining the inclination using only the measurement of the two GW polarizations.

There have been many studies looking at inclination constraints. From the GRB perspective these studies are largely divided into two groups. One focuses on exploring the possibility of nailing down the viewing angle by comparing the rate of GRB sources observed in GWs with those in gamma-rays (Williamson et al. 2014; Clark et al. 2015; Williams et al. 2018). The other focuses on measurements for individual detections, mainly in cases where the event has been three-dimensionally localized by an EM counterpart (Seto 2007; Arun et al. 2014). In Chen et al. (2018), it was observed that the inclination measurement is poor for binaries with an inclination of less than seventy degrees when there is no redshift information. They attribute this to a combination of the degeneracy between distance and inclination and the prior on the distance. Here, we explore the origin of the degeneracy in detail and discuss the importance of an additional degeneracy when the binary is circularly polarized (Fairhurst 2018).

Inclination constraints have also been discussed in the context of distance estimates for cosmology (Marković 1993; Nissanke et al. 2010; Chen & Holz 2013) and as part of wider parameter estimation investigations (Cutler & Flanagan 1994; Veitch et al. 2012; Narikawa et al. 2017; Vitale & Whittle 2018). It was noted in Nissanke et al. (2010) that adding detectors to a network did not seem to greatly improve the inclination measurement. Here, we investigate the extreme case: a network that measures both polarizations equally, as would be expected over the majority of the sky for the ET (Punturo et al. 2010).

2. Measuring Distance and Inclination

2.1. Origin of the Degeneracy

The degeneracy between distance and inclination arises directly from the dependence of the gravitational waveform on these parameters and has been discussed several times previously (Marković 1993; Cutler & Flanagan 1994; Nissanke et al. 2010). The GW signal, $h(t)$, incident on a GW detector, is (Ahorne 1987)

$$h(t) = F_+(\alpha_s, \delta_s, \chi)h_+(t) + F_\times(\alpha_s, \delta_s, \chi)h_\times(t), \quad (1)$$

where F_+ and $F_\times$ are the detector response to the plus and cross polarizations, respectively. The detector responses depend on the location (α_s, δ_s) of the source, where we have used subscripts to distinguish the right ascension of the source α_s from a later use of α to represent the alignment factor—a networks' relative sensitivity to the second polarization. In addition, we must specify a polarization angle χ to fully specify the *radiation frame*. It is common (Klimenko et al. 2005; Harry & Fairhurst 2011) to define a dominant polarization frame, for which the detector network is maximally sensitive to the plus polarization. With this choice, we can naturally characterize the network by its overall sensitivity and the relative sensitivity to the second polarization (Klimenko et al. 2005; Mills et al. 2018). This simplifies the comparison of different networks.

For a waveform where it is appropriate to neglect higher-order modes and precession, the two polarizations given in Equation (1) can be expressed in terms of the two orthogonal phases of the waveform:

$$h_+(t) = \mathcal{A}^1 h_0(t) + \mathcal{A}^3 h_{\frac{\pi}{2}}(t), \quad (2)$$

$$h_\times(t) = \mathcal{A}^2 h_0(t) + \mathcal{A}^4 h_{\frac{\pi}{2}}(t), \quad (3)$$
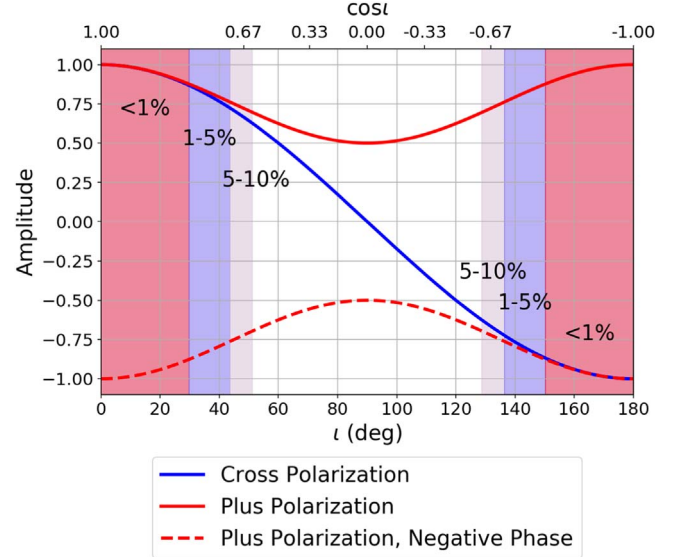

Figure 1. Relative contributions of the plus and cross polarizations of a gravitational-wave signal, dependent on the inclination. The red solid line indicates the amplitude of the plus polarization, while the dashed red solid line indicates the amplitude for the plus polarization with a negative phase. The blue solid line indicates the amplitude of the cross polarization. The shaded regions show the percent differences between the plus and cross polarizations. The red portion represents when the plus and cross polarization are less than 1% different. The blue region represents where the polarizations are between 1% and 5% different. The gray region represents where the polarizations are between 5% and 10% different.

where $\widetilde{h}_{\frac{\pi}{2}}(f) = i\widetilde{h}_0(f)$. The $\mathcal{A}^i$ are overall amplitude parameters, and depend on the distance d_L, inclination ι, polarization ψ, and coalescence phase ϕ_0 (Bose et al. 2000; Cornish & Porter 2007):

$$\mathcal{A}^1 = \mathcal{A}_+ \cos 2\phi_0 \cos 2\psi - \mathcal{A}_\times \sin 2\phi_0 \sin 2\psi, \quad (4)$$

$$\mathcal{A}^2 = \mathcal{A}_+ \cos 2\phi_0 \sin 2\psi + \mathcal{A}_\times \sin 2\phi_0 \cos 2\psi, \quad (5)$$

$$\mathcal{A}^3 = -\mathcal{A}_+ \sin 2\phi_0 \cos 2\psi - \mathcal{A}_\times \cos 2\phi_0 \sin 2\psi, \quad (6)$$

$$\mathcal{A}^4 = -\mathcal{A}_+ \sin 2\phi_0 \sin 2\psi + \mathcal{A}_\times \cos 2\phi_0 \cos 2\psi, \quad (7)$$

where $\mathcal{A}_+$ and $\mathcal{A}_\times$ are amplitudes for the plus and cross polarizations in the *source frame*, which is aligned with the binary's orbital angular momentum. They are given by

$$\mathcal{A}_+ = \frac{d_0}{d_L} \frac{1 + \cos^2 \iota}{2}, \quad (8)$$

$$\mathcal{A}_\times = \frac{d_0}{d_L} \cos \iota, \quad (9)$$

where d_L is the luminosity distance and d_0 is the reference luminosity distance. The variation of the two polarization amplitudes with inclination ι is shown in Figure 1. We note that there is an arbitrary choice of the *radiation frame* and this will affect the value of the angles ψ and χ and consequently the values of $\mathcal{A}^i$. However, the signal observed at the detectors is independent of this choice.

In principle, we should be able to measure all four of the amplitude parameters by accurately measuring both the amplitude and phase of both the plus and cross polarizations of a GW. From here, we could then infer the distance and orientation of the source binary. However, degeneracies limit our ability to accurately measure these parameters.
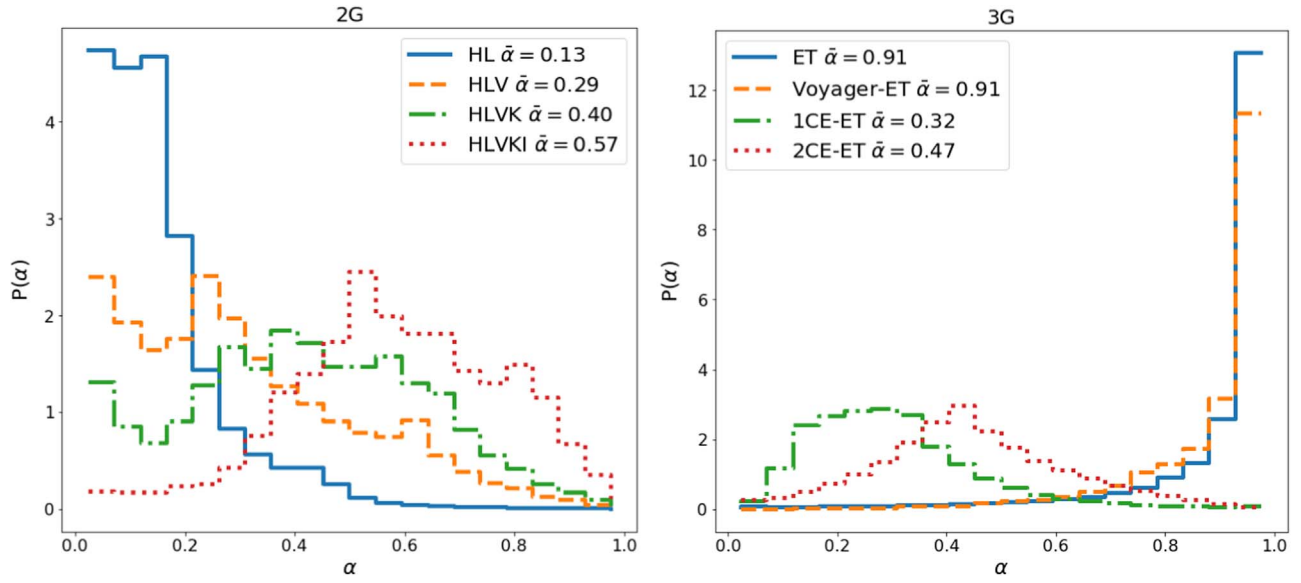
Figure 2. Relative sensitivity of detector networks to the second polarization, as encoded in the parameter α, defined through $F_\times = \alpha F_+$ (in the dominant polarization frame where the network is maximally sensitive to the plus polarization). The left plot shows the expected distribution of α for second-generation gravitational-wave networks, while the right plot shows the distribution for potential third-generation networks. In both cases, the distribution is the expected normalized distribution for a population of events, distributed uniformly in volume, and observed above the threshold in the detector network. Thus, directions of good network sensitivity are more highly weighted. In the legends, $\bar{\alpha}$ denotes the mean α for each network. The second-generation networks considered are LIGO Hanford and Livingston (HL); two LIGO detectors and Virgo (HLV); LIGO-Virgo and KAGRA (HLVK); and LIGO-Virgo-KAGRA with LIGO-India (HLVKI). As more detectors are added to the network, the average sensitivity to the second polarization increases. The right plot shows results for the Einstein Telescope (ET), which is comprised of three 60-degree interferometers, ET and three LIGO-Voyager detectors (Voyager-ET), and ET with either one or two Cosmic Explorer detectors (1CE–ET and 2CE–ET). As the ET detector has good sensitivity to both polarizations, networks where ET is the most sensitive detector will have large values of α. Third-generation target noise curves are taken from Abbott et al. (2017g).

In order to identify the inclination of the binary system using the polarizations of the GW, we must distinguish the contributions of the plus and cross polarizations. When the binary system is near face-on or face-away, the two amplitudes $\mathcal{A}_+$ and $\mathcal{A}_\times$ have nearly identical contributions to the overall GW amplitude. In Figure 1, we see that the relative difference between plus and cross is less than 1% for inclinations less than 30° (or greater than 150°) and 5% for inclinations less than 45° (or greater than 135°). This is the main factor that leads to the strong degeneracy in the measurement of the distance and inclination.

2.2. Network Sensitivity

As we have already described, GW detectors with limited sensitivity will preferentially observe signals that are close to face-on or face-off. In addition, when the binary is close to face-on and the emission is circularly polarized, the waveform is described by a single overall amplitude and phase (as the two polarizations are equal, up to a phase difference of ±90°). Thus it is no longer possible to measure both the polarization ψ and phase at coalescence ϕ_0 of the binary, but only the combination $\phi_0 \pm \psi$ (with the ± for face-on/away binaries respectively). This degeneracy, combined with the distance prior, leads to a significantly larger volume of parameter space, which is consistent with face-on, rather than edge-on systems.

To exclude face-on binaries from a marginalized posterior probability distribution on the inclination, the network must accurately measure the amplitude and phase of both of the polarizations. In general, GW detectors are not equally sensitive to the two polarizations. For a given sky location, we choose a plus and cross polarization such that the detector network most sensitive to the plus polarization and the remaining orthogonal component becomes the cross polarization. We can think of this as a detector network comprised of a long plus-detector and a shorter cross-detector (with a fraction α the length of the arms of the plus-detector). Thus, we can estimate the proportional sensitivity to the second polarization, called the network alignment factor (Klimenko et al. 2005), through the relation $F_\times = \alpha F_+$, where α varies between 0 and 1. Therefore, the sensitivity of the network to the second polarization can be determined by looking at the values of α over the sky.

Figure 2 shows the distribution of alphas for various detector networks. As might be expected, the sensitivity to the second polarization increases as more detectors are added to the network. For the two LIGO detectors, the typical value is $\alpha \sim 0.1$ because the two detectors have very similar orientations. When the Virgo detector is added to the network, the mode is $\alpha \sim 0.3$ and this increases to $\alpha \sim 0.5$ when KAGRA and LIGO-India join the network. The Einstein telescope (ET) is a proposed future detector with a triangular configuration (Punturo et al. 2010). For an overhead source, ET is equally sensitive to both polarizations, giving $\alpha = 1$. While ET does not have equal sensitivity to both polarizations over the whole sky, the majority of signals will be observed with $\alpha > 0.9$. For the future networks, we consider an ET detector complemented by either the advanced LIGO detectors with sensitivity improved by around a factor of three (LIGO-Voyager), or by one or two Cosmic Explorer (CE) detectors (Abbott et al. 2017g; Mills et al. 2018). When the ET detector dominates the network's sensitivity, we have excellent measurement of both polarizations, but in the CE–ET networks where CE is more sensitive, the relative sensitivity to the second polarization is comparable to the current networks.

2.3. Parameter Estimation

When a GW signal is observed in the data from the LIGO and Virgo instruments, the goal is to obtain estimates for the parameters that describe the waveform. Typically, Bayesian inference (Christensen et al. 2004; Rover et al. 2006; Veitch et al. 2015) is used to obtain a posterior distribution for the parameters of the system θ given the observed data d. As described in detail in Maggiore (2008), the likelihood of obtaining data d given the presence of a signal $h(\theta)$ and under the assumption of Gaussian noise characterized by a power spectrum $S(f)$ is

$$\Lambda(d|\theta) \propto \exp\left[-\frac{1}{2}(d - h(\theta)|d - h(\theta))\right]. \quad (10)$$

Here, we have introduced the weighted inner product

$$(a|b) := 4\,\mathrm{Re}\int_0^{f_{\max}} \frac{\tilde{a}(f)\tilde{b}(f)^\star}{S(f)}\,df. \quad (11)$$

The likelihood for a network of detectors is simply the product of likelihoods for the individual detectors:

$$\Lambda(d|\theta) \propto \exp\left[-\frac{1}{2}\sum_{i\in\mathrm{dets}}(d_i - h_i(\theta)|d_i - h_i(\theta))\right]. \quad (12)$$

The posterior distribution for parameters θ given the data d is given as

$$p(\theta|d) \propto \Lambda(d|\theta)p(\theta), \quad (13)$$

where $p(\theta)$ is the prior distribution for the parameters. The posterior distributions are typically calculated by performing a stochastic sampling of the distribution (Christensen & Meyer 2001; Christensen et al. 2004; Rover et al. 2006; van der Sluys et al. 2008a, 2008b). Distributions for a subset of parameters are obtained by marginalizing, or integrating out, the additional parameters.

In this analysis, we are interested in obtaining the joint distribution of the luminosity distance d_L and binary inclination ι. This is calculated as

$$p(d_L, \cos\iota|d) = \int d\mu \Lambda(d|\mu, d_L, \cos\iota)p(\mu, d_L, \cos\iota). \quad (14)$$

Typically, μ contains all parameters describing the system, including the masses, spins, sky location, orientation, and parameters describing the nuclear equation of state. For our work, we consider a simplified model, for which the only additional parameters contained in μ are the binary's polarization ψ and coalescence phase ϕ_0. We choose uniform priors on these parameters, as well as a uniform prior on $\cos\iota$, which leads to a uniform distribution of binary orientation. Furthermore, we use a uniform-in-volume prior for the distance $p(d_L) \propto d_L^2$. For binaries at greater distance, we need to take into account cosmological effects and use a prior with sources uniform in comoving volume and merging at a constant local rate. At even greater distances, the local merger rate would follow the star formation rate (Madau & Dickinson 2014), which peaks at redshift $z \sim 2$. We take this into account later in this paper for BBH systems, which can be detected throughout the universe with future detectors.

In our approximation, we fix the sky location and arrival time of the signal, as well as the masses and spins of the system. Fixing the sky location is reasonable, as one of the main motivations for this work is to investigate the accuracy of GW measurements of distance and inclination after the signal has already been identified and localized by the detector network. We also investigate how inclination measurements from GW observations can be combined with electromagnetic observations. An unknown sky location will only lead to larger uncertainties in the distance and inclination measurements arising from varying detector sensitivities over the sky.

While the masses and spins of the binary will not be known, in most cases these parameters have little impact on the inferred distance and inclination. This is especially true for low mass systems such as binary neutron stars which typically have component masses in the range 1.2–1.6$M_\odot$ (Özel et al. 2012; Pejcha et al. 2012). These systems are in-band for a large number of cycles, $\mathcal{O}(10^4$–$10^6)$, allowing the accurate measurement of the phase evolution of the binary. In these cases the chirp mass M—the parameter determining the leading order phase evolution—is measured with great precision. Therefore, though M also appears in the amplitude, the uncertainty in M will be negligible relative to the total uncertainty in the amplitude and can be safely ignored when considering uncertainties in the measurement of the distance and inclination. For higher-mass binaries such as BBHs, typically fewer cycles of the waveform are visible $\mathcal{O}(10^1$–$10^3)$. This results in a less precise measurement of the binary chirp mass. This extra uncertainty in the overall amplitude will widen the posteriors on both the distance and inclination. The estimates here should thus be seen as best-case, and any extra uncertainty in mass and sky position will simply widen the posteriors. In the analysis presented here, we focus only on the dominant GW emission at twice the orbital frequency. For unequal-mass systems, the other GW harmonics can significantly affect the waveform, particularly when the binary has a high mass ratio, i.e., one of the compact objects is significantly more massive than the other (Capano et al. 2014). This can lead to improvements in the measurement of the binary orientation (London et al. 2018).

Spins that are misaligned with the orbital angular momentum lead to precession of the binary orbit (Apostolatos et al. 1994), which in principle can lead to an improved measurement of the binary orientation. To date, there is no evidence for precession in the observed GW signals (Abbott et al. 2016b, 2017b, 2017c, 2017d, 2017f), so the approximations discussed here would therefore be applicable. Furthermore, neutron stars observed to merge within a Hubble time (Burgay et al. 2003; Stovall et al. 2018) are not expected to achieve a spin high enough to have observable precession within ground-based detector bandwidths (Apostolatos et al. 1994; Abbott et al. 2018).

To verify that fixing the masses and spins has a limited impact on the recovered distance and inclination, we compare results from our model with those from the full parameter estimation of GW170817. We recreate the posterior distribution for the multi-messenger signal GW170817, with and without distance information from the coincident electromagnetic signal, and compare it to the full, Bayesian parameter estimation, with a fixed sky location, using the observed LIGO and Virgo data (Abbott et al. 2018). The results are shown in Figure 3. To generate our results, we approximate the data d by a GW signal at a distance of $d_L = 40.7$ Mpc (Cantiello et al. 2018) and an inclination of 153° (Abbott et al. 2018). We then generate a posterior distribution for the four-dimensional
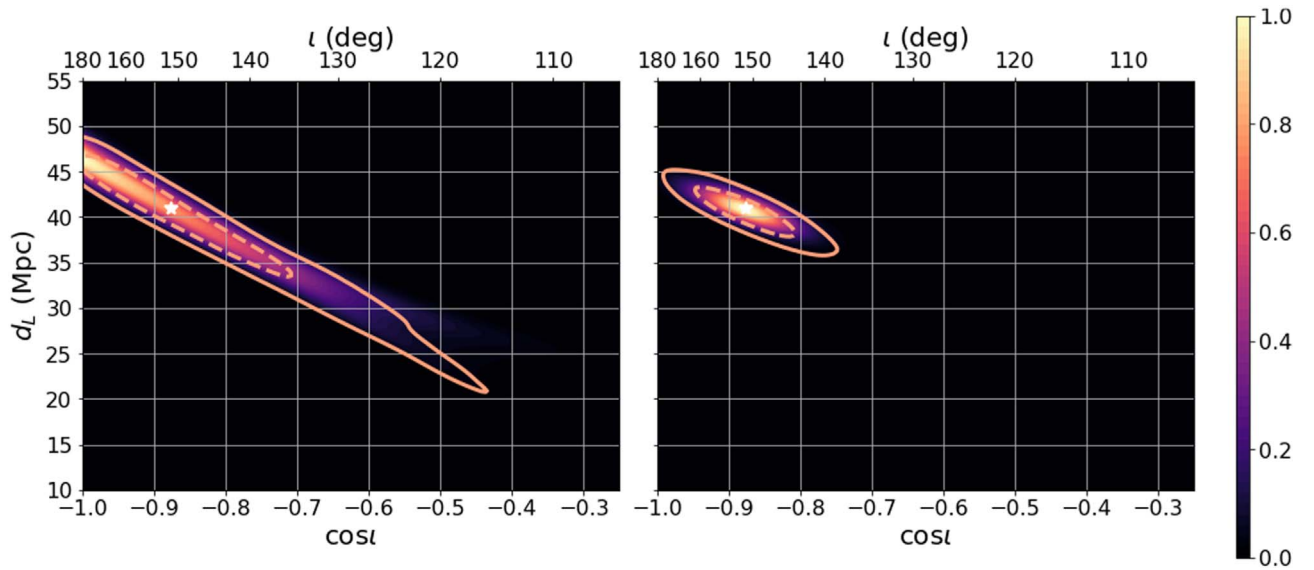
Figure 3. Marginalized posterior distribution for the distance and inclination of the binary neutron star system GW170817, detected with a signal-to-noise ratio $\rho \sim 32$ and network alignment factor $\alpha \sim 0.13$. The left plot was generated using only the data from gravitational-wave detectors, while the right plot also uses the independent distance measurement (40.7 Mpc, ± 2.4 Mpc at 90% confidence) from electromagnetic observations. The colored portion of the plot shows the probability distribution obtained using our approximate analysis, normalized such that the peak probability is 1. The orange contours represent the 90% and the 50% confidence intervals obtained by performing the full analysis of the LIGO-Virgo data (posterior samples are publicly available here: https://dcc.ligo.org/LIGO-P1800061/public; Abbott et al. 2018).

parameter space of distance d_L, inclination ι, polarization ψ, and coalescence phase ϕ_0. From this, we calculate the posterior distribution $p(d_L, \cos \iota | \mathbf{d})$, by marginalizing over the polarization and phase angles. As is clear from the figure, our approximate method gives a posterior on distance and inclination that is in excellent agreement with the full results from the real data.[1]

The results in Figure 3 show an example of the degeneracy in the measured values of the distance and binary inclination. The 50% confidence interval includes both a face-away binary at a distance of 45 Mpc and a binary inclined at $135°$ at a distance of 35 Mpc. It is only when the GW data are combined with the electromagnetically determined distance 40.7 ± 2.4 Mpc (Cantiello et al. 2018) that the binary inclination can be accurately inferred.

3. Accuracy of Measuring Distance and Inclination

Now that we understand how the degeneracy between inclination and distance arises, we can explore the expected accuracy with which these parameters will be measured in various GW detector networks. For concreteness, in the examples that follow, we fix the signal-to-noise ratio (S/N), denoted ρ, of the signals to be 12. While this might seem low, we note that for a detection threshold of 8, the *mean* S/N observed from a uniform-in-volume population would be 12 (Schutz 2011). We discuss higher S/N signals later in the paper. Rather than specifying a network and sky location, we instead investigate the ability to measure distance and inclination as we vary the network's relative sensitivity to the

second polarization, encoded in the variable α. For convenience, we fix the masses of the system to be $1.4 M_\odot$ and set the sensitivity of the detector network to the plus polarization of GW to be equal to that of a single advanced LIGO detector at the designed sensitivity for an overhead source. This places a face-on system at approximately 300 Mpc at S/N of 12. For inclined systems, the distance will be smaller to ensure that the network still receives an S/N of 12. While we have fixed the masses and detector sensitivities to make the plots, the results are essentially independent of these choices, up to an overall rescaling of the distance. Thus the results will be applicable to any system for which it is reasonable to neglect precession effects and the impact of higher modes in the gravitational waveform.

Let us begin by considering a network with relatively poor sensitivity to the second GW polarization, with $F_\times = 0.1 F_+$. This is typical for the LIGO Hanford–Livingston network and is common for the LIGO-Virgo network, as described in Figure 2. We consider two signals, both with an S/N of 12, but one that is face-on ($\iota = 0$) at a distance of 300 Mpc while the second is edge-on ($\iota = 90°$) at a distance of 150 Mpc, and has a polarization angle of $\psi = 0$ so that the GW power is contained in the plus polarization. The first column of figures in Figure 4 shows the likelihood across the distance–inclination plane. Here, we simply kept the values of ϕ_0 and ψ equal to zero, the value used in generating the signal. Note that the contours here are calculated for our simplified model and do not represent the results of full parameter estimation analyses, as they did in Figure 3. As expected, the maximum likelihood occurs at values of distance and inclination that exactly match the signal. We observe a degeneracy in distance and inclination, so that there is some support for the edge-on binary to be face-on (or face-away). There is also degeneracy for the face-on binary, which is marginally consistent with an edge-on binary, but face-away orientation can be excluded. With an S/N of 12 and $\alpha = 0.1$, for a face-on signal we expect an S/N of about 1.2 in the cross polarization. These results show that the presence or

---

[1] We note that the results in Abbott et al. (2018) show this distribution as a function of inclination ι instead of $\cos \iota$. This leads to a different distribution, and different 90% confidence intervals, as these are defined to be the minimum range that contains 90% of the probability, and this is dependent upon variable choice. As we discuss later, there is no evidence in the GW data alone that the signal is not face-off, and because the prior is flat in $\cos \iota$ we believe that plotting the distribution against $\cos \iota$ leads to a clearer understanding of the distribution.
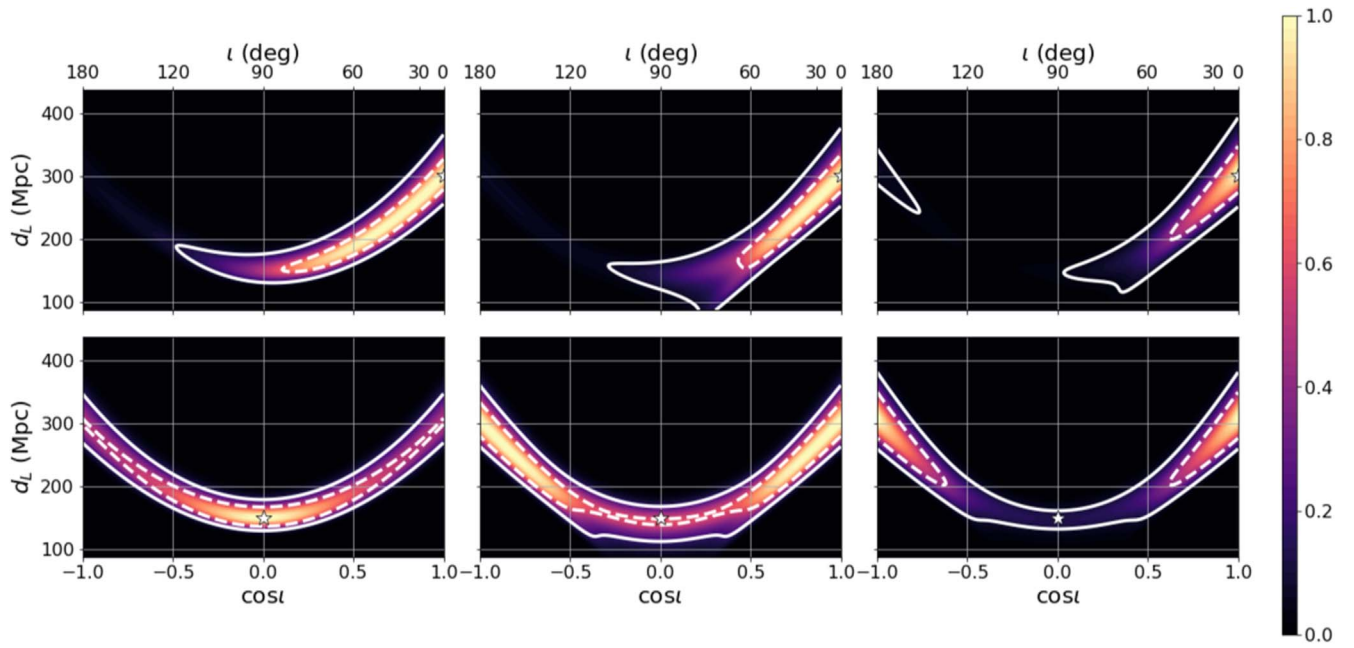
Figure 4. Progression of the probability distributions over a $\cos\iota$ and distance parameter space for a signal detected with alignment factor $\alpha = 0.1$ and S/N $\rho = 12$. The white star represents the injected signal. The top panel shows the distribution for a face-on signal. The bottom panel shows the distribution for an edge-on signal. The leftmost plots are the distribution for *only* the likelihood. This is generated by calculating the S/N fall off over the parameter space. Since we have not yet marginalized over the phase ϕ_0 and polarization ψ, the orientation angles are set equal to the values used in the injection, in this case zero for both ϕ_0 and ψ. The middle plots show how these distribution change when marginalizing over ψ and ϕ_0. Lastly, the rightmost plots are the complete probability distribution, calculated by applying a distance-squared weighting to the likelihood. This is to account for the expectation that binary systems are distributed uniformly in volume. Recall that $\alpha = 0.1$ is the mode sensitivity for the Hanford-Livingston network. The white star represents the hypothetical signal. The white contours represent the 50% and 90% confidence intervals obtained from our simplified model. Note that these contours do not represent the results of full parameter estimation, as they did in Figure 3. From these plots, we can see that at this α, a side-on signal is indistinguishable from a face-on/face-away signal.

absence of this signal is sufficient to down-weight, but not exclude, an edge-on orientation when the source is really face-on, and vice-versa. For a face-away system, the expected signal in the cross polarization is the same amplitude, but entirely out of phase from the face-on system, and this is sufficient to distinguish the two.

In the second column, we show the likelihood marginalized over the polarization and phase angles. This marginalization does not have a significant impact on the face-on binary, but completely changes the distribution for the edge-on binary— with the marginal likelihood now peaked at $\cos\iota = \pm 1$. Typically, we would expect to be able to measure the two phase angles with accuracy $\sim 1/\rho$, thus to a crude approximation, marginalizing over the phase angles would give a contribution $\approx (1/\rho^2)\Lambda_{\max}$, where $\Lambda_{\max}$ is the maximum likelihood. When the binary is recovered (nearly) face-on, the two amplitudes $\mathcal{A}_{+,\times}$ are (nearly) equal. Consequently, the signal is circularly polarized, with the phase determined by $\phi_0 + \psi$. Changing the value of $\phi_0 - \psi$ has no effect on the waveform. Thus, when marginalizing over the polarization and phase, we obtain a factor $\sim (\pi/\rho)\Lambda_{\max}$. Thus, for this signal at S/N 12, marginalizing the polarization and phase will lead to a relative increase of nearly 40 in favor of the face-on signal.

Finally, in the third column, we include the distance prior by re-weighting by d_L^2 to place sources uniformly in volume. This gives an additional factor of four weighting in favor of the face-on signal over the edge-on one. Once all these weightings are taken into account, the probability distributions between a face-on and edge-on signal are similar for a network with this sensitivity. The edge-on signal has slightly more support at $\cos\iota \approx 0$, and this is still included at 90% confidence. Additionally, the edge-on signal is consistent with either a

face-on or face-away orientation. It may seem strange that we will not recover the parameters of the edge-on system accurately. However, this is appropriate. As we have discussed, the volume of parameter space consistent with a face-on system is significantly larger than that for the edge-on case. Thus, even if we observe a signal that is entirely consistent with an edge-on system, it is more likely that this is due to a face-on system and noise fluctuations leading to the observed signal than it is that the signal is coming from an edge-on system. We note that this effect is also seen in Narikawa et al. (2017). Their Figures 4–6 show two LIGO detectors recovering edge-on systems as face-on or face-away, which results in the wrong sky location being measured.

Our next example investigates differing inclinations for a signal detected by a network with an $F_\times = 0.5 F_+$, i.e., a network with half the sensitivity to the cross polarization as the plus polarization. This is the predicted mean sensitivity expected for the best near-future detector network consisting of the Hanford, Livingston, Virgo, KAGRA, and LIGO-India detectors. Again, the S/N is set to 12 for all hypothetical signals, and now we consider three different inclinations: $\iota = 0$ (face-on) and two inclined signals, one with $\iota = 66°$, and the other with $\iota = 78°$. In Figure 5, we show the posterior distribution for distance and inclination for the three cases. Here, we have marginalized over the phase angles and included the distance prior weighting, so the plots are equivalent to the third column of plots in Figure 4.

The leftmost plot shows the probability distribution for a face-on signal. This distribution is similar to the one for $\alpha = 0.1$, though now the most inclined and face-away points in parameter space are excluded from the 90% credible region. The second plot is for a binary inclined at $66°$ ($\cos\iota = 0.4$).
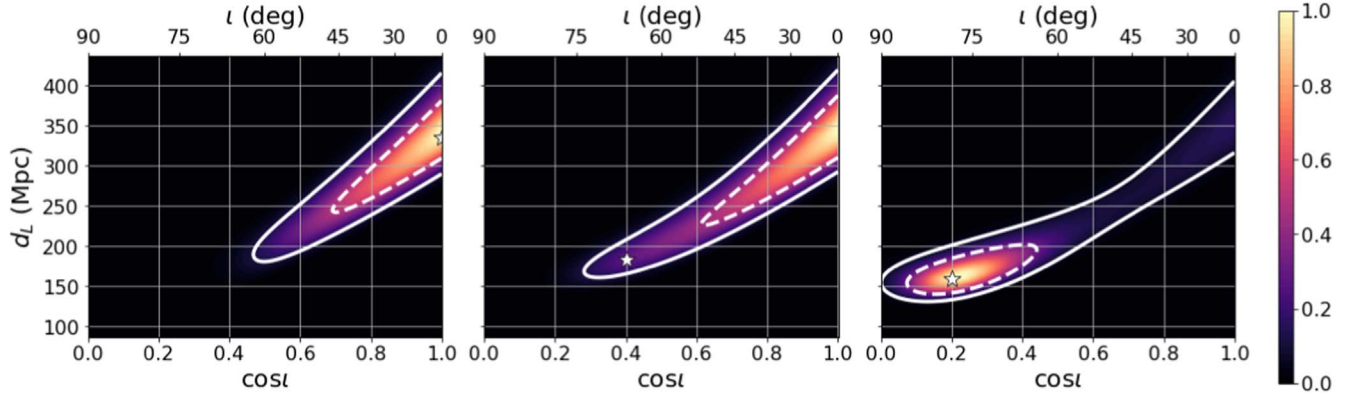
Figure 5. Probability distribution over a $\cos\iota$ and distance parameter space for a signal detected with alignment factor $\alpha = 0.5$ and S/N $\rho = 12$. The white star represents the injected signal. The white contours represent the 50% and 90% confidence intervals obtained from our simplified model. Note that these contours do not represent the results of full parameter estimation, as they did in Figure 3. A face-on signal (where $\cos\iota = 1$) returns a nearly identical probability distribution of the parameter space as a signal from a binary with an inclination of about 66 degrees ($\cos\iota = 0.4$). For inclinations in the range $0.1 < \cos\iota < 0.4$, though the distribution now peaks at the correct inclination, there is support extending across from face-on to an inclination of $\iota \sim 80° - 90°$. In these cases it is not possible to distinguish the binary inclination. The signal is only clearly identified as *not* face-on after $\cos\iota < 0.1$.

Table 1
Ability of Various Networks to Distinguish the Orientation of a Population of Binary Mergers with Given Inclination, ι

Network	$0° \leqslant \iota < 45°$			$45° \leqslant \iota < 60°$			$60° \leqslant \iota < 75°$			$75° \leqslant \iota < 90°$		
	Face-on	Uncertain	Inclined	Face-on	Uncertain	Inclined	Face-on	Uncertain	Inclined	Face-on	Uncertain	Inclined
HL	100%	0%	0%	97%	3%	0%	80%	18%	2%	47%	32%	21%
HLV	100%	0%	0%	86%	13%	1%	47%	44%	9%	29%	27%	44%
HLVK	100%	0%	0%	78%	21%	1%	27%	59%	14%	17%	20%	63%
HLVKI	100%	0%	0%	67%	32%	1%	7%	72%	21%	7%	13%	80%

Note. For each network and range of ι, we give the percentage of binaries for which the posterior on the inclination peaks at $\iota = 0°$ or $180°$ (face-on) and this peak contains over 90% of the probability; those binaries for which the recovered inclination peaks at the correct value, and greater than 90% of the probability is consistent with this peak (inclined); and those for which the posterior includes significant contributions for both face-on and inclined orientations (uncertain). For all networks, essentially all binaries with $\iota < 45°$ will be recovered face-on. As the inclination increases further, the ability to clearly identify the binary as inclined increases significantly with the number of detectors in the network, as this improves the average sensitivity to the second gravitational-wave polarization.

Here, the peak of the inclination distribution corresponds to a face-on system and indeed the posterior is nearly identical to that obtained for the face-on system. Thus, for a typical system with a close-to-threshold S/N we will remain unable to distinguish between face-on signals and those inclined at 60° based on GW observations alone. The best near-future detector therefore would be unable to measure a difference in inclination between these two hypothetical signals. For inclinations in the range $0.1 < \cos\iota < 0.4$ the 90% credible region includes peaks at both the true inclination and face-on. In this region, we cannot tell if the difference in polarization amplitudes arises from an inclined signal or from a signal with parameters in the much larger, and prior-preferred, volume of parameter space near face-on, with a noise fluctuation giving rise to the observed data. For values of $\cos\iota < 0.1$, the posterior is peaked at the correct value of ι and excludes face-on from the 90% credible region.

The results shown in Figures 4 and 5 show the general features of the distance and inclination distribution. It is characterized by three components: one consistent with a face-on signal, one with a face-off signal, and a third contribution peaked around the true values of distance and inclination. In all of the cases we have shown, only one or two of the contributions are significant. There are, however, cases where we obtain three distinct peaks in the posterior for the inclination, although these are rare. In Appendix B of Fairhurst (2018), an approximate expression for probability associated

with each peak was obtained, which is valid for networks sensitive to a range where a d_L^2 prior is still appropriate. This provides an analytic expression for the probability associated with each of the three contributions, as a function of S/N, inclination, polarization, and the network sensitivity to the second polarization, encoded in the variable α.

To get a sense of how accurately binary inclination will be measured, we simulated a set of 1,000,000 events isotropically and uniformly in both volume and orientation, keeping only those that would be observed above the detection threshold of the network (typically leaving 30,000–80,000 events). For each event, we then determined whether the event would be recovered as definitely face-on—over 90% of the probability associated with the face-on (and face-away) components of the distribution— or definitely inclined or uncertain. These results are summarized in Table 1, for a series of networks each with an increasing number of detectors. For all networks, essentially all events with a true inclination less than 45° will be recovered face-on. Only for those events with inclination greater than 45° do we start to be able to distinguish the orientation. Between 45° and 60°, networks with three or more detectors will classify a small fraction of events as inclined, and this fraction increases with both the inclination of the system and the number of detectors (which directly effects the typical value of α). However, even for events that have an inclination greater than 75°, the LIGO Hanford–Livingston network would recover half as face-on and only 20% as definitely not. This improves for
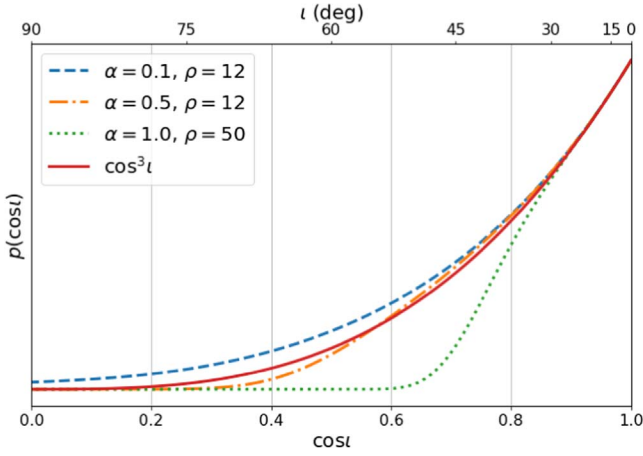
Figure 6. Un-normalized marginalized posterior for $\cos\iota$ for a face-on source as measured for three networks with alignment factors $\alpha = 0.1$, $\alpha = 0.5$, $\alpha = 1.0$, and signal-to-noise ratio $\rho = 12$, $\rho = 12$, $\rho = 50$, respectively. The solid line shows the expected $\cos^3\iota$ form of the likelihood.

the five-detector network where less than 10% are face-on and 80% are clearly identified as being inclined. We note that similar results have been obtained independently in Chen et al. (2018).

Next, let us consider the general accuracy with which we can measure the inclination for a binary that is (nearly) face-on. In this case, the distribution for the inclination angle can be approximated in a simple way. If we begin by assuming that the degeneracy between distance and inclination is exact, then orientations with $|\cos\iota| \approx 1$ are preferred due to the prior on the distance. This can be clearly seen by comparing the second and third columns of plots in Figure 4. The distribution in the second column (when we do not apply the uniform-in-distance weighting) shows a broad degeneracy with equal probability along lines of constant $\mathcal{A} = \cos\iota/d_L$. It is only by applying the distance re-weighting that the peak shifts more to $\cos\iota = 1$. We can obtain the posterior probability for a fixed value of ι by integrating over a given distribution, $p(\cos\iota/d_L)$:

$$p(\cos\iota) = \int d_L^2 p(\cos\iota/d_L)\,dd_L$$
$$\propto \int \cos^3\iota \,\mathcal{A}^{-4} p(\mathcal{A})\,d\mathcal{A}$$
$$\propto \cos^3\iota. \qquad (15)$$

Thus, it follows that where the degeneracy holds, the posterior on $\cos\iota$ will be proportional to $\cos^3\iota$. In Figure 6, we show the posterior for three examples of face-on signals : S/N $\rho = 12$ with $\alpha = 0.1$ and 0.5, and S/N $\rho = 50$ with $\alpha = 1$. All three distributions follow the $\cos^3\iota$ distribution for small inclinations. The high-S/N signal deviates at around 30°—at this inclination there is enough difference from a circularly polarized signal for larger inclinations to be disfavored. However, for the lower-S/N signals (and also lower values of α) the approximation remains accurate to greater than 45°.

We can improve the approximation by noting (Fairhurst 2018) that the S/N lost by projecting an inclined signal onto a circular signal is

$$\Delta\rho^2 = \frac{\alpha^2\rho^2}{(1+\alpha^2)^2}\frac{(1-\cos\iota)^4}{4}. \qquad (16)$$

This loss in S/N leads to a reduction in the likelihood associated with the inclined signal, which causes the
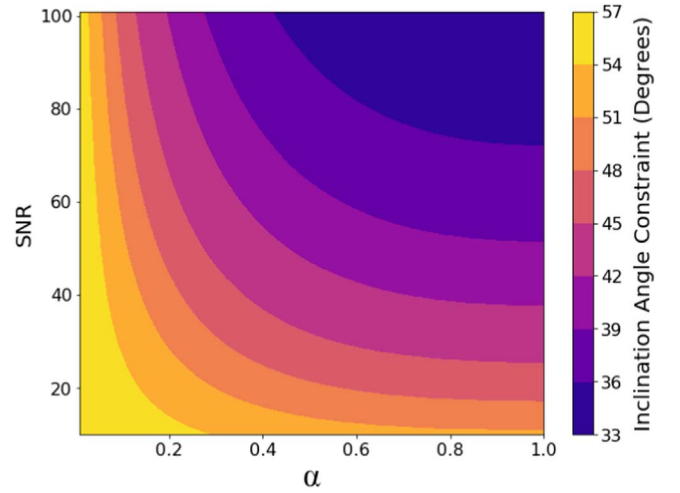

Figure 7. This plot shows a detector network's ability to constrain the inclination of a face-on signal with 90% confidence. The x-axis shows the network alignment factor α, whereas the y-axis shows the signal-to-noise ratio (S/N) of the hypothetical gravitational-wave signal. The color represents the upper limit on the inclination angle. For weak signals or for networks that are not very sensitive to the cross polarization, the network can only constrain the inclination to being less than about 45°. Even for the most sensitive detector network detecting the loudest hypothetical signals, the network would be unable to constrain the inclination to being less than 30°. However, we note that at these S/Ns, the detector network may be able to identify higher-order modes, which would break the degeneracy between distance and inclination, allowing more precise measurement of the inclination.

probability distribution to fall off more rapidly away from $\iota = 1$. In particular, we obtain

$$p(\cos\iota) \propto \cos^3\iota \exp\left(-\frac{\Delta\rho^2}{2}\right). \qquad (17)$$

We can use this expression to determine how well a network with sensitivity α would be able to constrain a signal's inclination ι given the S/N of the signal. In Figure 7, we specifically look at how tightly we can constrain a face-on signal. We can see that for low-S/N signals or for networks with little sensitivity to the cross polarization, GW observations will only be able to constrain the signal to being less than about 45°. Even with an extremely loud signal and a very sensitive detector network, we are only able to constrain the signal to about 30°. This effect has also been observed in the results of full parameter estimation runs in Vitale & Whittle (2018) where even with a network of two ETs and for sources nearby (at redshifts $z < 3$), the median 90% credible interval for the cosine of the inclination was found to be $\Delta\cos\iota \sim 0.15$, which at face-on corresponds to an inclination constraint of 30°. It is important to note here that at these S/Ns, higher-order modes or precession in the GW signal may be observable. If these were detected, the degeneracy between distance and inclination would be broken, and we would be able to more tightly constrain the inclination.

Finally, it is interesting to consider what effect the inclination-distance degeneracy would have on the mass estimate of BBHs. GW detectors actually measure the redshifted mass $M_{\rm det} = (1+z)\mathcal{M}_{\rm source}$, where the subscripts denote detector frame and source frame, respectively (Cutler & Flanagan 1994). There is no way to determine the redshift directly from the gravitational waveform of a BBH. However,
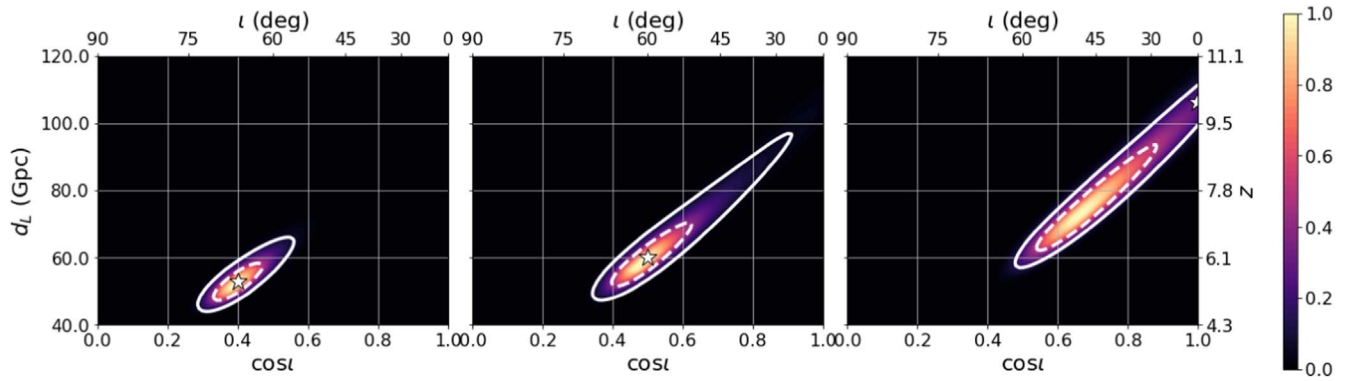
Figure 8. Marginalized posterior distribution for a $10M_\odot$–$10M_\odot$ BBH at redshift $z = 10$ detected by the Einstein Telescope in the most sensitive part of the sky, i.e., directly above the detector. Here, the alignment factor is $\alpha = 1$ and the S/N is $\rho = 20$. The white star represents the injected signal at three different inclinations: $\iota = 66°$, $\iota = 60°$ and $\iota = 0°$. The white contours represent the 50% and 90% confidence intervals obtained from our simplified model. Note that these contours do not represent the results of full parameter estimation, as they did in Figure 3. We use a prior that is uniform in comoving volume with a rest-frame rate density that follows the star formation rate (Madau & Dickinson 2014). At this redshift the prior varies by a factor of ∼12 across the degeneracy and now favors more inclined binaries. Thus, binaries that are face-on will be recovered as being more inclined. The redshift uncertainty $\Delta z/z \sim 40\%$ dominates the statistical error in the recovery of the binary chirp mass. All conversions between luminosity distance and redshift assume standard cosmological parameters (Ade et al. 2016).

the measured value of the luminosity distance can give the redshift if a cosmology is assumed. In this way, the inclination-distance degeneracy will map to an uncertainty in the rest-frame masses. For the next generation of GW detectors that will be sensitive to BBH mergers throughout the universe, the uncertainty in the redshift will likely be the dominant uncertainty in the masses. As such, we explore the inclination measurement with ET for a BBH merger at a redshift of $z = 10$ with intrinsic masses of $10M_\odot$ each, corresponding to a detector frame chirp mass of $\mathcal{M}_{\mathrm{det}} = 96M_\odot$. We place the source directly above the detector, in the most sensitive part of the sky. In this case, $\alpha = 1$ and $\rho = 20$, where we have assumed standard cosmology (Ade et al. 2016).

At these cosmological distances, a d_L^2 prior for the distance is no longer appropriate. Rather, we use a distance prior that is uniform in comoving volume, where the rest-frame binary merger rate density follows the cosmic star formation rate (Madau & Dickinson 2014) with a delay between star formation and binary merger Δt, and a distribution of delay times $p(\Delta t) \propto 1/\Delta t$ (Totani 1997; see Section 5 of Mills et al. 2018 for details). The new prior peaks at $z \sim 1.4$. Therefore at $z \sim 10$, the nearer, more inclined binaries are a priori more likely.

In Figure 8, we show the marginalized posterior for three different inclinations: $\iota = 66°$, $\iota = 60°$, and $\iota = 0°$. For the second-generation networks in Figure 5, the $\iota = 66°$ ($\cos\iota = 0.4$) source is recovered as face-on. With the higher S/N and improved sensitivity to the second polarization, ET can identify the signal as edge-on. At an inclination of $\iota = 60°$, the degeneracy still extends across $25° < \iota < 70°$, though smaller inclinations are now excluded from the 90% credible interval. This is the effect of the new distance prior, which is a factor of 12 larger at redshift 6 than at redshift 10. Thus, though the 90% credible region of the marginalized likelihood extends right up to face-on, the prior is able to partially break the degeneracy. For less inclined binaries $\iota < 60°$, the 90% probability interval extends up to face-on.

For the face-on binary in the rightmost plot, the prior shifts the peak of the posterior away from the true value. Although the value of the likelihood at face-on and redshift 10 is a factor of 12 larger than it is at an inclination of $60°$ and redshift 6, these two points in the parameter space are equally likely after

the prior re-weighting. If the detector frame chirp mass of the binary is measured to be $\mathcal{M}_{\mathrm{det}} = 96M_\odot$, the degeneracy between the inclination and distance results in $\mathcal{M}_{\mathrm{source}} = 96M_\odot$ and $\mathcal{M}_{\mathrm{source}} = 61M_\odot$ being equally likely. The detector-frame chirp mass $\mathcal{M}_{\mathrm{det}}$ would be determined to an accuracy similar to the accuracy of the GW phase measurement $\Delta\mathcal{M}_{\mathrm{det}}/\mathcal{M}_{\mathrm{det}} \sim 1/(\rho \mathcal{N}_{\mathrm{cycles}})$ (Finn & Chernoff 1993; Nissanke et al. 2010). Parameter estimation for GW150914 yielded a precision in the detector-frame mass estimate of $\Delta\mathcal{M}_{\mathrm{det}}/\mathcal{M}_{\mathrm{det}} \sim 10\%$ for a comparable S/N Abbott et al. (2016c). Everything else being equal, GW150914 with a detector frame chirp mass of $\mathcal{M}_{\mathrm{det}} \sim 30M_\odot$ will have more cycles than the ET binary with detector-frame chirp mass $\mathcal{M}_{\mathrm{det}} = 96M_\odot$ above say 20 Hz. However, ET's improved sensitivity at low frequencies compared to LIGO means that we can expect the precision of the detector-frame mass estimate of GW150914 and the ET binary to be roughly the same. Thus, the broad uncertainty in the intrinsic masses due to the distance-inclination degeneracy $\Delta\mathcal{M}_{\mathrm{source}}/\mathcal{M}_{\mathrm{source}} \sim 40\%$ will dominate the total error budget.

4. Conclusion and Future Work

Our work demonstrates that even with a network equally sensitive to both polarizations of the GW, we would be unable to precisely measure the inclination or distance of a nearly face-on binary due to a strong degeneracy between distance and inclination. However, we have focused on non-spinning binaries and assume that the sky location, masses, and arrival times of the detectors are all known. Introducing these parameters would increase the uncertainties. Exploring how these parameters affect the overall measurement of the distance and inclination could give a more accurate summary of a GW network's ability to measure distance and inclination.

The degeneracy between inclination and distance described here could be broken in a few different ways: by using distance or inclination from electromagnetic measurements, by detecting higher-order modes (London et al. 2018), and by measuring precession (Vitale & Chen 2018). Binary neutron star systems produce a variety of EM signatures, as were observed for GW170817 (Abbott et al. 2017e). Neutron star-black hole binaries (NSBHs) could produce EM signatures should the neutron star be tidally disrupted. However, tidal disruption only

happens at relatively small mass ratios (Pannarale et al. 2015). For larger mass ratios, the neutron star falls into the black hole before tidal disruption can produce EM signatures. Interestingly, both precession and higher modes have a larger effect on the gravitational waveform at higher mass ratios (Kidder 1995; Varma et al. 2014). The polarizations of the higher modes have a different dependence on the inclination, and the precession of the orbital plane would result in changing amplitudes for the plus and cross polarizations. These effects can make it easier to identify the inclination angle (Varma et al. 2014; Graff et al. 2015; Calderón Bustillo et al. 2016; London et al. 2018; Vitale & Chen 2018). For NSBHs, the degeneracy can thus be broken by either information from the EM emission or from higher modes or precession. Vitale & Chen (2018) demonstrated that precession would break the distance–inclination degeneracy in NSBH for a few binaries with a few values of the precession angle and large, highly spinning black holes. It would be an interesting follow-up to this study to explore this with a realistic distribution of spins, to see when precession plays a significant role in measuring binary parameters.

ORCID iDs

S. A. Usman ⓘ https://orcid.org/0000-0003-0918-7185
J. C. Mills ⓘ https://orcid.org/0000-0002-0808-7804
S. Fairhurst ⓘ https://orcid.org/0000-0001-8480-1961

References

Abbott, B. P., Abbott, R., Abbott, T. D., et al. 2016a, PhRvL, 116, 061102
Abbott, B. P., Abbott, R., Abbott, T. D., et al. 2016b, PhRvX, 6, 041015
Abbott, B. P., Abbott, R., Abbott, T. D., et al. 2016c, PhRvL, 116, 241102
Abbott, B. P., Abbott, R., Abbott, T. D., et al. 2017a, Natur, 551, 85
Abbott, B. P., Abbott, R., Abbott, T. D., et al. 2017b, PhRvL, 118, 221101
Abbott, B. P., Abbott, R., Abbott, T. D., et al. 2017c, ApJL, 851, L35
Abbott, B. P., Abbott, R., Abbott, T. D., et al. 2017d, PhRvL, 119, 141101
Abbott, B. P., Abbott, R., Abbott, T. D., et al. 2017e, ApJL, 850, L40
Abbott, B., Abbott, R., Abbott, T. D., et al. 2017f, PhRvL, 119, 161101
Abbott, B. P., Abbott, R., Abbott, T. D., et al. 2019, PhRvX, 9, 011001
Abbott, B. P., Abbott, R., Abbott, T. D., et al. 2017g, CQGra, 34, 044001
Ade, P. A. R., Aghanim, N., Arnaud, M., et al. 2016, A&A, 594, A13
Apostolatos, T. A., Cutler, C., Sussman, G. J., & Thorne, K. S. 1994, PhRvD, 49, 6274
Arun, K. G., Tagoshi, H., Mishra, C. K., & Pai, A. 2014, PhRvD, 90, 024060
Aso, Y., Michimura, Y., Somiya, K., et al. 2013, PhRvD, 88, 043007
Blair, D. G., Barriga, P., Brooks, A. F., et al. 2008, Journal of Physics: Conference Series, 122, 012001
Bose, S., Pai, A., & Dhurandhar, S. V. 2000, IJMPD, 9, 325
Burgay, M., D'Amico, N., Possenti, A., et al. 2003, Natur, 426, 531
Calderón Bustillo, J., Husa, S., Sintes, A. M., & Pürrer, M. 2016, PhRvD, 93, 084019
Cantiello, M., Jensen, J. B., Blakeslee, J. P., et al. 2018, ApJL, 854, L31
Capano, C., Pan, Y., & Buonanno, A. 2014, PhRvD, 89, 102003
Chen, H.-Y., & Holz, D. E. 2013, PhRvL, 111, 181101

Chen, H.-Y., Vitale, S., & Narayan, R. 2018, arXiv:1807.05226
Christensen, N., Libson, A., & Meyer, R. 2004, CQGra, 21, 317
Christensen, N., & Meyer, R. 2001, PhRvD, 64, 022001
Clark, J., Evans, H., Fairhurst, S., et al. 2015, ApJ, 809, 53
Cornish, N. J., & Porter, E. K. 2007, CQGra, 24, 5729
Cutler, C., & Flanagan, É. E. 1994, PhRvD, 49, 2658
De, S., Finstad, D., Lattimer, J. M., et al. 2018, PhRvL, 121, 091102
Fairhurst, S. 2018, CQGra, 35, 105002
Farr, W. M., Stevenson, S., Coleman Miller, M., et al. 2017, Natur, 548, 426
Finn, L. S., & Chernoff, D. F. 1993, PhRvD, 47, 2198
Finstad, D., De, S., Brown, D. A., Berger, E., & Biwer, C. M. 2018, ApJL, 860, L2
Goldstein, A., Veres, P., Burns, E., et al. 2017, ApJL, 848, L14
Graff, P. B., Buonanno, A., & Sathyaprakash, B. S. 2015, PhRvD, 92, 022002
Guidorzi, C., Margutti, R., Brout, D., et al. 2017, ApJL, 851, L36
Harry, I., & Fairhurst, S. 2011, PhRvD, 83, 084002
Kidder, L. E. 1995, PhRvD, 52, 821
Klimenko, S., Mohanty, S., Rakhmanov, M., & Mitselmakher, G. 2005, PhRvD, 72, 12202
London, L., Khan, S., Fauchon-Jones, E., et al. 2018, PhRvL, 120, 161102
Madau, P., & Dickinson, M. 2014, ARA&A, 52, 415
Maggiore, M. 2008, Gravitational Waves (Oxford: Oxford Univ. Press)
Mandel, I. 2018, ApJL, 853, L12
Marković, D. 1993, PhRvD, 48, 4738
Metzger, B. D. 2017, arXiv:1710.05931
Mills, C., Tiwari, V., & Fairhurst, S. 2018, PhRvD, 97, 104064
Narikawa, T., Kaneyama, M., & Tagoshi, H. 2017, PhRvD, 96, 084067
Nissanke, S., Holz, D. E., Hughes, S. A., Dalal, N., & Sievers, J. L. 2010, ApJ, 725, 496
Özel, F., Psaltis, D., Narayan, R., & Villarreal, A. S. 2012, ApJ, 757, 55
Pannarale, F., Berti, E., Kyutoku, K., Lackey, B. D., & Shibata, M. 2015, PhRvD, 92, 084050
Pejcha, O., Thompson, T. A., & Kochanek, C. S. 2012, MNRAS, 424, 1570
Punturo, M., Abernathy, M., Acernese, F., et al. 2010, CQGra, 27, 084007
Roulet, J., & Zaldarriaga, M. 2019, MNRAS, 484, 4216
Rover, C., Meyer, R., & Christensen, N. 2006, CQGra, 23, 4895
Sathyaprakash, B., Fairhurst, S., & Schutz, B. 2013, Scientific Benefits of Moving one of LIGO Hanford Detectors to India, Tech. Rep. T1200219, Alexandria, VA: NSF , https://dcc.ligo.org/LIGO-T1200219/public
Schutz, B. F. 1986, Natur, 323, 310
Schutz, B. F. 2011, CQGra, 28, 125023
Seto, N. 2007, PhRvD, 75, 024016
Stovall, K., Freire, P. C. C., Chatterjee, S., et al. 2018, ApJL, 854, L22
Tanvir, N. R., Levan, A. J., Gonzalez-Fernandez, C., et al. 2017, ApJL, 848, L27
Thorne, K. 1987, in 300 years of Gravitation, ed. S. Hawking & W. Israel (Cambridge: Cambridge Univ. Press), 330
Tiwari, V., Fairhurst, S., & Hannam, M. 2018, ApJ, 868, 140
Totani, T. 1997, ApJL, 486, L71
van der Sluys, M., Raymond, V., Mandel, I., et al. 2008a, CQGra, 25, 184011
van der Sluys, M. V., Roever, C., Stroeer, A., et al. 2008b, ApJL, 688, L61
Varma, V., Ajith, P., Husa, S., et al. 2014, PhRvD, 90, 124004
Veitch, J., Mandel, I., Aylott, B., et al. 2012, PhRvD, 85, 104045
Veitch, J., Raymond, V., Farr, B., et al. 2015, PhRvD, 91, 042003
Villar, V. A., Guillochon, J., Berger, E., et al. 2017, ApJL, 851, L21
Vitale, S., & Chen, H.-Y. 2018, PhRvL, 121, 021303
Vitale, S., & Whittle, C. 2018, PhRvD, 98, 4029
Williams, D., Clark, J. A., Williamson, A. R., & Heng, I. S. 2018, ApJ, 858, 79
Williamson, A. R., Biwer, C., Fairhurst, S., et al. 2014, PhRvD, 90, 122004